Spring 2022

Bond Valence Sum Analysis on Compounds Prepared by Topochemical Manipulation

Yasmin Dayeh

Bond Valence Sum Analysis on Compounds Prepared by Topochemical Manipulation

By

Yasmin Dayeh

PROJECT

Submitted in partial fulfillment of the requirements

for the degree of Master of Science in Analytical Chemistry

Governors State University

University Park, IL

May 2022

Advisor: Dr. K. G.Sanjaya Ranmohotti

Acknowledgments

I am highly indebted to my advisor, Dr. K. G.Sanjaya Ranmohotti, for his guidance, both on a personal and professional levels during my time in this program. This project would not have been possible without his constant supervision as well as for providing necessary information regarding the project and for his support in completing the project. I would like to extend my sincere thanks to the committee members, Dr. Walter Henne and Dr. Joong-Won Shin for taking the time to review this project as well as for their constant guidance and commitment to share their vast knowledge for the past two years in this program. I would also like to acknowledge the Computer and IT Services department at Governors State University for assisting me with repairing issues and accessing the CrystalMaker software utilized in this project. I would like to express my gratitude towards my parents for their support and encouragement in whatever I pursue. My thanks and appreciations also go to my colleagues whom I met and worked with during this time in the program, and to my coworkers at Harold Washington College. In particular, the Project Laboratory Coordinator, Jessica Gorogianis, for her cooperation and flexibility to work around my school schedule, which helped me complete the requirement for this program and complete this project.

TABLE OF CONTENTS

LIST OF FIGURES

LIST OF TABLES

Abstract

The Bond Valence theory of Brown (1978) has been extensively used to correlate metal oxidation state to coordination environment in solids. Although the bond valence sum (BVS) appears to be extremely useful to coordination chemists, it has not often been applied as an alternative measure of refinement quality. In this work, previously reported six layered perovskite compounds including, $RbLaNb_2O_7$, $Rb_2LaNb_2O_7$, $Rb_2S_xLaNb_2O_7$ ($x \leq 0.8$), $NaLaNb_2O_7$, $(Cs_2Cl)LaNb_2O_7$, and $(FeCl)LaNb_2O_7$, that have been prepared by topochemical manipulation and their structures have been determined by Rietveld refinements were analyzed. Our focus was to explore whether the determination of oxidation state using the bond distances derived from the Rietveld refinement method could be used to validate structure determination along with the reported goodness of fit values, χ^2, in the published structure. Good agreement between the calculated and the expected oxidation states would provide support for the chemical formula and the accuracy of a crystal structure determination.

We applied the concept of the BVS method for selective metal ions including, niobium (Nb), lanthanum (La), rubidium (Rb), sodium (Na), cesium (Cs), sulfur (S), and iron (Fe). For all these metal ions, the final values resulted from BVS calculations for the six compounds overall showed good agreement between the calculated and the expected oxidation. Although this method is empirical, it can nevertheless help us to identify important trends when a series of related and similarly prepared samples are prepared.

Introduction

Crystal chemistry-the study of the crystal structure of chemical compounds- is a predominant field to coordination chemists and material scientists due to the crystal structure's importance in defining a compound's physical properties such as, the electrical, magnetic, and optical properties. Over the years, scientists have been conducting intensive studies investigating the crystal structure types of chemical compounds, their properties, and applications. These compounds, which have a significance use in industry, are known as the coordination compounds. Coordination compounds are composed of a metal cation in the center, and in some instances, the metal ion is composed of a transition metal.

Transition metals can acquire different oxidation states[1] that result in having coordination compounds of different structures. Hence, giving a compound a different physical property depending on the metal ion oxidation state. Before delving into a coordination compound's physical properties and potential application, one must explain how the oxidation state of transition metal is related to the compound's structure determination. This can be done by explaining the theory underlying the relation between bond lengths, bond valences, and structure determination known as the Bond Valance Sum (BVS) theory.

In 1971, the BVS model was introduced by scientists Ian David Brown and Bob Shannon.[2,3] Their work was based on Pauling's electrostatic valence concept for ionic structures that states that the sum of bond valences S_{ij} around any ion, i, is equal to its valence, V_i (i.e., the formal oxidation state).[4] This relation was expressed in equation (1).[5]

$$V_i = \Sigma S_i \quad (1)$$

Together with Bragg's electrical flux lines[6], Brown was able to develop an empirical model and further propose a mathematical expression, shown in equation (2)[5], that relates the bond

valance, oxidation state, and the bond length of a metal ion.[5] Hence, from this expression, the BVS model explains that the sum of the bond valence of an atom is equal to the atom's oxidation state, denoted by an *S*,[7]

$$V_{ij} = \Sigma S_{ij} = \Sigma \ exp[\frac{R_0 - rij}{b}] \quad \textbf{(2)}$$

where *Vij* is the oxidation state of atom *I*, S_{ij} is the bond valence and r_{ij} is the length of the bond formed between atoms *i* and *j*, and R_0 and *b*, are the bond valence parameters. R_0 and *b* represent the nominal length of a bond of valence unit (v.u.), which depends on the size of the atom forming the bond, and the softness of the interaction between the two atoms, respectively.[8]

Values for these two parameters are obtained by fitting the bond-valence-bond-length correlation to a set of well-defined chemical structures. Moreover, 141 reliable values for the parameter R_0 have been calculated for many metal-ligand combinations of different oxidation states using the Inorganic Crystal Structure Database (ICSD).[2,9,10] As for the bond valance parameter, *b*, it was refined to be equal to 0.37Å.[3] Tabulated values of R_0 and *b* can be acquired from the literature. For example, for the R_0 parameter for Nb^{4+}, Nb^{5+}, Rb^{+}, La^{3+}, Fe^{2+}, Fe^{3+}, Na^{1+}, and Cs^{+1} metal ions that are bonded to an oxygen in the (-2) oxidation state, were reported to be equal to 1.88, 1.911, 2.263, 2.172, 1.734, 1.759, 1.803, and 2.417, respectively. In addition, the reported R_0 parameter for sulfide, S^{2-} ion bonded to Rb^{+} is set to 2.7, while the reported R_0 parameter for Fe^{2+}, Fe^{3+}, and Cs^{1+} ions that are bonded to a chlorine anion were set to 2.06, 2.09, and 2.7, respectively.[5,8]

Applying the corresponding values for R_0 and *b* found in literature into equation 2, the sum of the individual values of the bond valance, S_{ij} around a central metal ion, gives the oxidation state value, V_{ij}. Therefore, the formal oxidation state of the metal ion can be easily determined using bond distances extracted from crystal structural information. For example, using the proper

R_0 and the *b* parameters, the BVS of an iron (Fe) metal ion in the (+2) oxidation state, will lead to a bond valence value (*S)* close to the integer two. Similar calculations applying the R_0 parameters for iron metal of a different oxidation state (e.g., +3 oxidation state), will give an *S* value close to its oxidation state, (e.g., close to integer three for Fe^{3+}).

Despite the BVS significance to coordination chemists, it has not been widely used in evaluating the oxidation state of metal ions.[8] This model can provide details on the oxidation states of the metal ions and services as an additional support for the accuracy of the crystal structure determinations. Moreover, the same approach can be applied to crystal structure determination by Rietveld analysis. Since the BVS model relates the bond lengths around a transition metal to its oxidation state,[11] our main interest will be focusing on analyzing whether the oxidation state of metal ions could be calculated using the bond distances obtained from the structure, which has been refined by Rietveld method.

In this study, the BVS of six Perovskite-type metal oxides prepared by topochemical manipulation and their structures have been determined by Rietveld refinements, will be surveyed. Moreover, to calculate the oxidation state of metal ions including, niobium (Nb), lanthanum (La), rubidium (Rb), Sodium (Na), Cesium (Cs), and Iron (Fe), using the bond distances, and to assess the proposed crystal structure determination. Both Nb and Fe adopt different valence, where Nb can adopt a +4 and, or +5 oxidation state, while Fe can adopt a +2 and, or +3 oxidation state. The oxidation state of La ion is +3 oxidations state, while Rb, Na, and Cs, all adopt a +1 oxidations state. Agreement between the calculated and the expected oxidation states for these six ions, would provide support for the chemical formula and the accuracy of a crystal structure determination. Before analyzing the BVS of the select Perovskite-type metal oxides for this study and, a brief overview of the Perovskite-type cell structure, the topochemical manipulation method of

preparation of solid-state compounds, and the Rietveld refinements for structural determination, will be outlined.

One crystal structure type that have significant properties and application in industry, is known as the layered Perovskite structure. Many materials exhibit a perovskite-type crystal structure. For example, the naturally occurring perovskite mineral with ionic conductivity property, known as calcium titanium oxide, $CaTiO_3$, exhibit a simple cubic perovskite cell structure that is made of made of double oxide mixture of calcium oxide and titanium oxide. This structure is unique due to exhibiting a wide range of electrical, magnetic, and optical properties depending on their composition.[12] The most common and simplest Perovskite, shown on the left in Figure 1, is composed of a primitive cubic unit cell, ABX_3, where A is an alkali metal, or an alkali-earth metal, B is a transition metal, and X is an anion.[12] Our study focuses on layered perovskite-type metal oxide, (Figure 1, right), with a structure composed of 2D layers of ABO_3 where each layer is separated by the metal cation denoted by, A. There are three types of layered perovskites including, the Dion-Jacobson (DJ) (with a formula, $(AA'_{n-1}B_nO_{3n+1},)$ where A: alkali metal, or an alkali-earth metal, A′: Lanthanides, B: transition metal, and n: thickness), the Ruddlesdon-Popper (RP) (with a formula, $(A_2A'_{n-1}B_nO_{3n+1})$), and the Aurivillius phase (AV).[13,14]

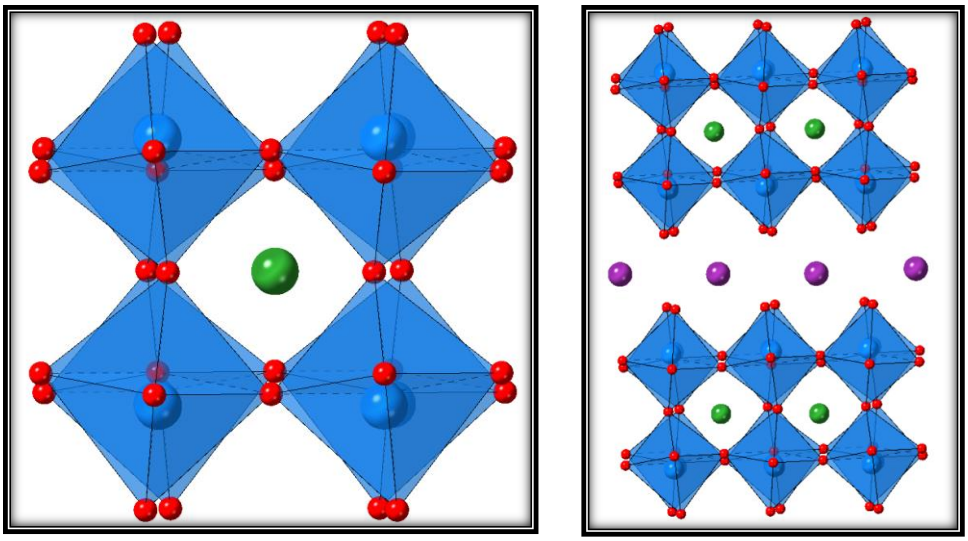

Figure 1. Three-dimensional cubic (left) and two-dimensional layered (right) perovskite structures generated using CrystalMaker.[15] The A' site is represented by the green sphere, the transition metal ion is represented by the blue (BO_6) octahedron environment, and the anion is represented by the red sphere. For the layered perovskite (Right), the A cation separates the two layers and is represented in purple spheres.

As stated earlier, a total of six previously reported layered perovskites were selected for this study. Moreover, these compounds have been synthesized by a method known as the topochemical manipulation method. The topochemical reaction strategies offer an important low temperature (< 500 °C) approach for the manipulation of various inorganic host materials while providing access to new compounds that cannot be prepared by standard high temperature methods. The key characteristic of topochemical manipulation is its ability to modify existing structural features while maintaining the basic structure of the host material. Thus, these reactions have been applied to several perovskite and perovskite-related compounds.[14]

Traditionally, many metal oxide materials have been prepared at very high temperatures to accelerate the slow solid-solid diffusion, resulting in the formation of thermodynamically stable phases at high temperatures. On the other hand, soft chemical reactions (i.e., topochemical reactions) such as, intercalation, deintercalation, and ion-exchange, have been performed at relatively low temperatures. Thus, making it useful for the synthesis of new metastable phases.

Soft-chemical reactions for the synthesis of inorganic materials has attracted much attention, particularly in terms of the search for new materials with interesting properties. This is mainly because acquiring an understanding of the nature of the reaction, can pave the way to utilize the topochemical manipulation effectively to tailor the properties of materials.

Furthermore, upon using topochemical reactions to prepare solid state materials, the structure determination of these compounds can be analyzed using X-ray and neutron diffraction and their structure can be determined by a method known as Rietveld refinement. X-ray and neutron diffraction are among the most powerful analytical techniques for probing the chemical structure in the solid state, and ranging from fundamental to the applied, they are widely employed in academic and industrial research. The breadth and importance of these techniques are exemplified by several databases. One is, the Cambridge Structural Database, which contains over 1,000,000 organic/organometallic entries that have been crystallographically characterized[16]; the Inorganic Crystal Structure Database (ICSD) which contains over 200,000 inorganic crystal structures[17]; and the International Centre for Diffraction Data's Powder Diffraction File (PDF)[18] which contains over 425,000 inorganic entries.

All substances consist of atoms. The types of atoms and their three-dimensional arrangement is what defines the structure of materials; thus, the nature of materials. Since the properties and functions of materials relate directly to its structure, there are extensive research for various materials such as high-temperature superconductors, batteries and energy materials, ferroelectric materials, zeolite chemistry, negative thermal expansion, pharmaceutical polymorphism, and many others. A single crystal of target material is necessary to conduct single crystal X-ray structure analysis, and an ordered, three-dimensional repetitive structure. That is, the best single crystal is one in which all molecules comprising the single crystal have the same steric

structure, and the geometrical arrangement of molecules within a unit cell is the same viewing from any direction. For viewing the three-dimensional structure of molecules quantitatively, it is required to satisfy the conditions such as (1) Types of atoms are distinguishable, (2) The position of the individual atom which is buried inside of the molecule can be determined even if the molecule is large like proteins, and (3) The view of molecules from as many different directions as possible can be obtained. In addition, the relative positions among the molecules from different view must be determined precisely. It is the X-ray crystallography that satisfies these conditions and currently it is the most popular analytical method to solve the three-dimensional structure of the molecule.[19]

Single-crystal X-ray Diffraction is an analytical technique which provides detailed information about the internal lattice of crystalline substances. Including, the unit cell dimensions, bond-lengths, bond-angles, and details of site-ordering. Directly related, is single-crystal refinement, where the data generated from the X-ray analysis is interpreted and refined to obtain the crystal structure. While single crystal diffraction is considered the gold standard for determination of crystal structures, this approach has some of its own distinct disadvantages: for many compounds, it can be difficult or impossible to grow diffraction-quality single crystals and it is frequently the case that actual single crystals are not ideal, and there may be irregularities. For instance, having more than one molecule in an asymmetric unit, multiple crystal domains (twinning), or the disordered structure Powder diffraction on the other hand has many of its own distinct advantages: samples can be readily studied under real working conditions, samples can be studied through phase transitions where single crystals would be destroyed, and multiphase samples can be studied allowing qualitative or quantitative phase analysis. [20]

For these reasons, powder diffraction[21] has often provided the crucial break through structural insights in diverse areas such semiconductor, electronic, food, pharmaceutical, or life science related materials. However, this method is not suitable in general for analyzing complicated organic compounds and large molecules, such as proteins, although there are reports on the crystal structure determination of proteins using the powder method.[22] The X-ray diffraction method is most suited to crystal structure determination if a single crystal that is large enough for the measurement is available. However, in many circumstances, samples are obtained only in the form of microcrystalline powders, which hinders the use of the single-crystal method and in such circumstances, the powder method is ideal.

Powder diffraction is one of the most widely used analytical techniques for characterizing solid state materials. The scanning of the powdered material leads to a powder diffraction pattern as a plot of diffracted intensity as a function of angle 2θ. When electromagnetic radiation with a wavelength comparable to interatomic separations is incident on a crystalline sample where each atom acts as a source of scattered radiation and the constructive/destructive interference between the scattered waves leads to diffraction. If we consider a crystal containing planes described by Miller indices (*hkl*), Bragg's law gives the angle of constructively scattered intensity via

$$\boldsymbol{\lambda = 2d_{hkl} \sin \theta} \qquad \textbf{(3)}$$

where λ is the wavelength, d_{hkl} is the interplanar spacing (d-spacing), and 2θ is the direction relative to the incident beam. The d-spacing is the perpendicular distance between any pair of adjacent planes in the set and it is the d_{hkl} value appears in Bragg's law. For any crystal system, d_{hkl} can be related to the unit-cell parameters a, b, c, α, β, γ by trigonometry. For a cubic unit cell, the (100) planes simply have a d-spacing of a, the value of the cell edge. For (200) in a cubic cell, d = a/2.[23] For a tetragonal unit cell (a=b ≠ c; α = β = γ = 90°), the general expression simplifies to

$$\frac{1}{d_{hkl}^2} = \frac{h^2+k^2}{a^2} + \frac{l^2}{c^2} \quad \textbf{(4)}$$

Furthermore, the angles of diffracted intensity ($2\theta_{hkl}$) in any diffraction pattern depend solely on the size and shape of the unit cell. For a single crystal, it leads to a beam of diffracted intensity in specific directions when Bragg's law is satisfied. When Bragg's law is satisfied, the reflected beams are in-phase and interfere constructively. At angles of incidence other than the Bragg angle, reflected beams are out-of-phase and destructive interference or cancellation occurs. In a traditional powder diffraction experiment, a detector is scanned across sample to produce a plot of diffracted intensity versus angle 2θ called a powder diffraction pattern. These patterns are normally treated as a series of intensity values, $y_{obs,I}$, at N discrete 2θ steps. The intensity I_{hkl} of each *hkl* reflection is determined by the identity and positions of the atoms inside the unit cell via the structure factor, F_{hkl}:

$$F_{hkl} = \sum_j t_j f_j exp\left[2\pi i\left(hx_j + ky_j + lz_j\right)\right] \quad \textbf{(5)}$$

$$I_{hkl} \propto |F_{hkl}|^2 \quad \textbf{(6)}$$

where, x_j, y_j, and z_j are fractional atomic coordinates of atom *j*, and f_j is the scattering factor of atom *j* as a function of sin θ/λ. The t_j term accounts for the fact that atoms vibrate around their average positions in real samples, which decreases I_{hkl} intensities.[24] In any real diffraction experiment, each *hkl* reflection is observed over a small range of 2θ values giving a peak of finite width. The shape of the peak is caused by a combination of effects from the radiation source, the diffractometer components, and the sample. [25]

The most commonly known disadvantage of powder diffraction is that the three-dimensional diffraction data of a single crystal is compressed onto the single dimension of the diffraction angle, 2θ, so that the different *hkl* reflections often overlap in 2θ. This overlap suggests

that, in contrast to single crystal methods, the experimental determination of the accurate intensities of individual reflections needed for structural analysis could be difficult or impossible.

One way to solve this problem is to adopt a whole-pattern fitting approach in which a structural model (a description of the peak shapes and parameters to describe the background), are used to calculate a powder pattern. The calculated intensity, $y_{\mathrm{calc},i}$, at each step in 2θ is then compared to the observed intensity $y_{\mathrm{obs},i}$. The difference between the two is then minimized by changing certain parameters of the model. This is commonly performed by a least-squares refinement.[26] There are a few other important whole-pattern fitting methods used in powder diffraction analysis. One can simply freely refine the 2θ values and intensities of peaks to describe each reflection without a structural model. This method can be used to determine unit-cell parameters in a process called auto indexing. Another is to adjust the intensity of each reflection except at 2θ values constrained by a unit cell and *hkl* indices. This approach enables us to decide the best fit possible to an experimental data set for a given unit cell. [27]

The first powder diffraction pattern was reported over a century ago.[28] For the first 50 years, the application of powder diffraction in structural analysis of materials was severely limited. This was because of the collapse of three-dimensional reciprocal space onto one-dimensional data sets leads to a severe reduction of information, caused by an accidental and systematic peak overlap. In 1969, Hugo Rietveld published the seminal article[29] on what has become known as the Rietveld refinement method. This method offers an elegant way to sidestep the problem of peak overlap. The underlying idea relies on modeling a calculated powder neutron diffraction pattern, described by a set of parameters. These parameters include various contributions to the pattern, such as the background, crystal lattice and symmetry, crystal structure, microstructure, instrumental factors, and others. All these parameters can be simultaneously refined by the least-

squares method, until the calculated pattern matches the experimentally collected data. Once a satisfactory match is achieved, the crystal structure is considered refined. [30]

The introduction of this technique was a significant step forward in the diffraction analysis of powder samples as, unlike other techniques at that time, it was able to deal reliably with strongly overlapping reflections. It is worth mentioning that it is required to have a starting structural model for Rietveld refinement in order to produce a reasonable initial calculated powder diffraction pattern[31] and the most common approach is to use an approximate structural model derived from a related compound. One can also start refinements from different random starting models and essentially solve the crystal structure from scratch and remarkably complex unknown structures have been solved with this type of approach.[32]

Diffraction data are a set of intensity values measured at a set of specific momentum transfer values, which are usually expressed as 2θ settings. By convention, the intensity values are labeled as $y_{O,i}$, where O indicates these are observed values and i indicates the intensity was measured at 2θ value $2\theta i$. To perform Rietveld analysis, it is required to have an uncertainty estimate for $y_{O,i}$ which can be defined as $\sigma[y_{O,i}]$. Earlier, this was called the estimated standard deviation (esd), but now crystallographic convention uses the term standard uncertainty (s.u).[33]

The intensity values simulated from the model are labeled as $y_{C,i}$, where the C indicates they are computed from the model. The Rietveld algorithm optimizes the model function to minimize the weighted sum of squared differences between the observed and computed intensity values, i.e., to minimize $\Sigma_i w_i (y_{C,i} - y_{O,i})^2$ where the weight, labeled as w_i , is $1/\sigma^2 [y_{O,i}]$.[34] The most straightforward discrepancy index, the weighted profile R-factor (R_{wp}), follows directly from the square root of the quantity minimized, scaled by the weighted intensities: $R^2_{wp} = \Sigma_i w_i (y_{C,i} - y_{O,i})^2$

/ $\Sigma_i w_i (y_{O,i})^2$. Another very useful concept is called the expected *R* factor (R_{exp}). Using *N* as a label for the number of data points, $R^2_{exp} = N/\Sigma_i w_i (y_{O,i})^2$.[35]

A related statistical concept is that of "Chi squared" or χ^2, which measures the goodness of fit obtained by Rietveld refinement analysis. It can be said that the model is ideal and s.u. values are correct, by considering that the expected value for $(y_{C,i} - y_{O,i})^2 / \sigma^2[y_{O,i}]$ will be one. The χ^2 term is defined as the average of these values, where $\chi^2 = (1/N) \Sigma_i w_i (y_{C,i} - y_{O,i})^2 / \sigma^2[y_{O,i}]$ and *N* is considered to be the number of data points.[35] It is important to note that χ^2 can also be determined from the expected and weighted profile *R* factors $\chi^2 = (R_{wp} / R_{exp})^2$. During the refinement process, χ^2 starts out large when the model is poor and decreases as the model produces better agreement with the data. Having a model where χ^2 is far from unity has a very profound implication with many modern Rietveld programs. Till the present, there have been many kinds of refinement software to be used for crystal structure refinement such as Fullprof, DBWS [36] and GSAS[37].

However, as with much of modern crystallography, the software used for Rietveld refinement is frequently treated as a "black box" that produces often poorly understood outputs. In some instances, when a large percentage of the total intensity in a pattern comes from background, then fitting the background alone can give relatively small χ^2 values, even without a valid structural model. [38] Some argue why it is not possible for someone to create a rule-of-thumb for at least one of them, where having a value above some threshold is a cause for suspicion, but a value below that threshold indicates a refinement that is generally reliable.[39]

Scientists mastering Rietveld refinement techniques commonly raise these questions such as what do the various Rietveld discrepancy values, i.e., χ^2 and *R* factors mean? What values allow one to distinguish good refinements from poor ones? These questions are important to people who review Rietveld results, as well as individuals trying to decide if the results that are reported in

literature are likely to be trustworthy knowing a guideline that can be used as an absolute measure of refinement quality. The most important indicator of the correctness of a Rietveld fit is the visual inspection of the match between the calculated and observed patterns.[38] All observed reflections should be explained by the model and their relative intensities correctly described. No unfitted extra reflections should be observed.

The bond valence is frequently used to validate newly determined crystal structures, but it has many other uses in the analysis and modelling of crystal structures. Therefore, our interest was to explore whether the determination of oxidation state using the bond distances derived from the Rietveld refinement method could be used as an alternative measure of refinement quality along with the reported χ^2 values (and other *R* factors) in the published structures. Expecting that good agreement between the calculated and the expected oxidation states, would provide support for the chemical formula and the accuracy of a crystal structure determination achieved by Rietveld analysis.

Calculation Section

For six previously reported layered perovskite compounds including, $RbLaNb_2O_7$, $Rb_2LaNb_2O_7$, $Rb_2S_xLaNb_2O_7$ ($x \leq 0.8$), $NaLaNb_2O_7$, $(Cs_2Cl)LaNb_2O_7$, and $(FeCl)LaNb_2O_7$, the bond length data for BVS calculation were derived by inserting the crystallographic information into CrystalMaker software[15], which is a user-friendly molecular and crystal structure visualization software. Moreover, the structure refinement of these has been aided by the Rietveld method using different software packages including, the GSAS[37]**,** the EXPGUI interface[40], TF14LS based on the Cambridge Crystallographic Subroutine Library[41], FullProf [42], and RIETAN on ACOS 2010 computer.[43] Rietveld refinement provides information as for the crystal-chemical changes, phase transition and quality of phases as well as for certain microstructural characteristics of the

investigated crystalline matter like the coherently diffracting domain sizes and the micro strain distribution. [40] Generally, the results of the structure refinement provide a list of x,y,z assignments for each atom in the unit cell, the distance of the nearest atomic neighbors and shape of the anisotropic intensity center for each atom (i.e., the thermal parameters). By using structural parameters such as, unit cell, space group, and atomic positions, the crystal structure of these size compounds were drawn in this study using CrystalMaker[15].

Results and Discussion

The first perovskite compound studied here is $RbLaNb_2O_7$ and structure of this compound has been refined by Rietveld method. The refinement has been converged to R_{wp} =6.9% and R_E =5.2%. The atomic coordinates and the thermal parameters for $RbLaNb_2O_7$ are listed in Table 1. Rietveld analysis conducted on neutron powder diffraction data shows that this phase crystallizes in an orthorhombic space group with *a* = 5.4941(4) Å, *b* = 21.9901(6) Å, and *c* = 5.4925(4); *Imma* (No. 74); *Z* = 4. Figure 2 shows the structure of $RbLaNb_2O_7$ where the perovskite layers are eclipsed, and the lower layer charge allows the Rb^+ to reside in a cubic site extended away from the perovskite block.[44]

Table 1. Atomic Coordinates and Equivalent Displacement Parameters for $RbLaNb_2O_7$

Atom	Wyckoff notation	x	y	z	Uiso (Å^2)[a]
Nb	8h	0	0.35274(9)	0.4990(7)	0.30(3)
La	4e	0.5	0.25	0.4921(10)	0.24(4)
Rb	4a	0	0	0	1.98(7)
O(1)	4e	0	0.25	0.4469(12)	1.29(13)
O(2)	8h	0	0.4325(2)	0.5469(8)	1.06(6)
O(3)	8g	0.25	0.3435(2)	0.25	1.72(8)
O(4)	8g	0.75	0.3275(2)	0.75	0.76(5)

a Uiso is the isotropic atomic displacement parameters obtained from Rietveld refinement.

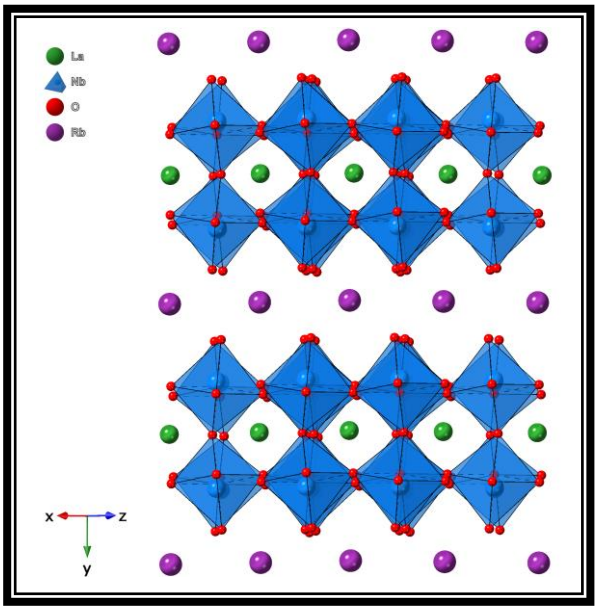

Figure 2. Structure of $RbLaNb_2O_7$. The octahedra represent NbO_6 and Nb-O bonds are shown. Green spheres represent La and purple spheres represent Rb.

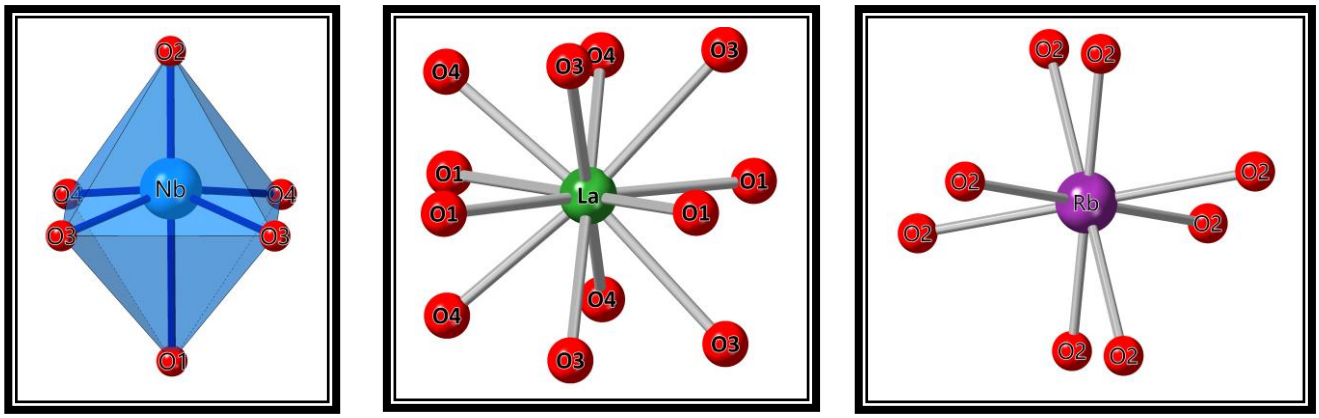

Figure 3. The niobium cation resides in a NbO_6 environment (left). The Lanthanum cation resides in a LaO_{12} environment (middle). The rubidium cation resides in a RbO_8 environment (right).

The niobium atoms in this compound are coordinated to six oxygens to form distorted octahedra. As shown in Table 2, Nb adopts bond distances normally observed in the Nb^{5+}. The Nb-O bond distances range from 1.782 Å to 2.272 Å and the average Nb-O distances in NbO_6 is 2.00 Å. Significantly close to the value of 1.99 Å obtained from the sum of the Shannon crystal

radii[45,46] for six coordinated Nb^{5+} (0.78 Å) and two-coordinated O^{2-} (1.21Å). In order to provide additional proof for this point and to eliminate the possibility of the occurrence of a Nb^{4+} ion, the BVS calculation was performed with the Nb-O bond lengths (in Table 2) obtained from the Crystalmaker structure. Moreover, the previously reported R_0 values extracted from literature for Nb^{4+} and Nb^{5+} that is 1.88 and 1.911, respectively, and b was set equal to 0.37 were applied.[2,5] An example of the calculation of the valence for the bond Nb-O(1) (bond length rNb(1)-O(1) = 2.272 Å) is as follows:

In the case of Nb^{5+}, $R_0 = 1.911$, $s = \exp[(R_0 - r\text{Nb-O(1)}/b] = 0.35$

In the case of Nb^{4+}, $R_0 = 1.88$, $s = \exp[(R_0 - r\text{Nb-O(1)}/b] = 0.38$

Similar calculations can be performed for other Nb-O bonds. The sum of the valences of the bonds around the Nb ion provide an estimation of its oxidation state. The result of the BVS calculations for Nb is summarized in Table 2. The sum of bond valences is 5.12 v.u. for Nb^{5+} and 4.71 v.u. for Nb^{4+} and these values are closer to the integer five. Thus, it is reasonable to assign that the Nb ion is in +5 oxidation state.

Table 2. Selected Bond Distances (Å) in NbO_6 octahedra, and Bond valence sum

Bond	**Bond length (Å)**	**Valence**	
		Nb^{4+}	**Nb^{5+}**
Nb-O(1)	2.272	0.35	0.38
Nb-O(2)	1.782	1.30	1.42
Nb-O(3) × 2	1.915	1.82	1.98
Nb-O(4) × 2	2.058	1.24	1.34
	Sum	4.71	5.12

The lanthanum atoms in this compound are coordinated to twelve oxygens to form a distorted polyhedra. As shown in Table 3, La adopts bond distances normally observed in the La^{3+}. The La-O bond distances range from 2.400 Å to 3.093Å and the average La-O distances in LaO_{12} is 2.72 Å. Significantly agrees with the value 2.71 Å obtained using the sum of the Shannon crystal radii[45,46] for twelve coordinated La^{3+} (1.50 Å) and two-coordinated O^{2-} (1.21Å). The BVS calculation was performed with the La-O bond lengths (in Table 3) obtained from the Crystalmaker structure. Moreover, the previously reported R_0 values extracted from literature for La^{3+} (i,e., 2.172), and the *b* was set equal to 0.37, were applied.[2,5] The result of the BVS calculations for La is summarized in Table 3, where the sum of bond valences was found to be 2.97 v.u. This value is close to the integer three. Thus, it is reasonable to assign that the La ion is in +3 oxidation state.

Table 3. Selected Bond Distances (Å) in LaO_{12} units, and Bond valence sum

Bond	**Bond length (Å)**	**Valence** La^{3+}
La-O(1)	2.400	0.54
La-O(1)	3.093	0.08
La-O(1) × 2	2.757	0.41
La-O(3) × 4	2.802	0.73
La-O(4) × 4	2.614	1.21
	Sum	2.97

The rubidium atoms in this compound are coordinated to eight oxygens to form distorted polyhedra. As shown in Table 4, Rb adopts bond distances normally observed in the Rb^{+}. The Rb-O bond distances range from 2.898 Å to 3.351Å and the average Rb-O distances in RbO_8 is 3.13

Å. This comparable with 2.96 Å, the sum of the Shannon crystal radii[45,46] for eight coordinated Rb^+ (1.75 Å) and two-coordinated O^{2-} (1.21Å). The BVS calculation was performed with the Rb-O bond lengths (in Table 4) obtained from the Crystalmaker structure. Moreover, the previously reported R_0 values extracted from literature for Rb^+ (i.e., 2.263), and *b* was set equal to 0.37, were applied.[2,5] The result of the BVS calculations for Rb is summarized in Table 4, where the sum of bond valences was found to be 0.85 v.u. This value is close to the integer one. Thus, it is reasonable to assign that the Rb ion is in +1 oxidation state.

Table 4. Selected Bond Distances (Å) in RbO_8 units, and Bond valence sum

Bond	**Bond length (Å)**	**Valence** Rb^+
Rb-O(2) × 2	2.898	0.36
Rb-O(2) × 4	3.133	0.38
Rb-O(2) × 2	3.351	0.11
	Sum	0.85

The second perovskite oxide compound studied was $Rb_2LaNb_2O_7$ and structure has been refined by Rietveld method. The refinement has been converged to R_{wp} =3.9% and R_E =1.2%. The atomic coordinates and the thermal parameters for $Rb_2LaNb_2O_7$ are listed in Table 5. Rietveld analysis conducted on neutron powder diffraction data shows that this phase crystallizes in an orthorhombic space group with *a* = 22.30955(9) Å, *b* = 5.69748(10) Å, and *c* = 5.69365(10); *Cmmm* (No. 63); *Z* = 4. Figure 4 shows the structure of $Rb_2LaNb_2O_7$ where the perovskite layers are staggered.[44]

Table 5. Atomic Coordinates and Equivalent Displacement Parameters for $Rb_2LaNb_2O_7$

Atom	Wyckoff notation	x	y	z	Uiso ($Å^2$)[a]
Nb	8g	0.09369(4)	0.2475(4)	0.75	0.185(12)
La	4c	0	0.2603(5)	0.25	0.38(2)
Rb	8g	0.19197(5)	0.7387(4)	0.75	0.68(3)
O(1)	4c	0	0.7018(6)	0.25	1.17(6)
O(2)	8g	0.17616(6)	0.7691(5)	0.25	0.78(2)
O(3)	8e	0.08704(7)	0.5	0.5	0.60(2)
O(4)	8e	0.07368(6)	0	0.5	0.36(2)

a Uiso is the isotropic atomic displacement parameters obtained from Rietveld refinement.

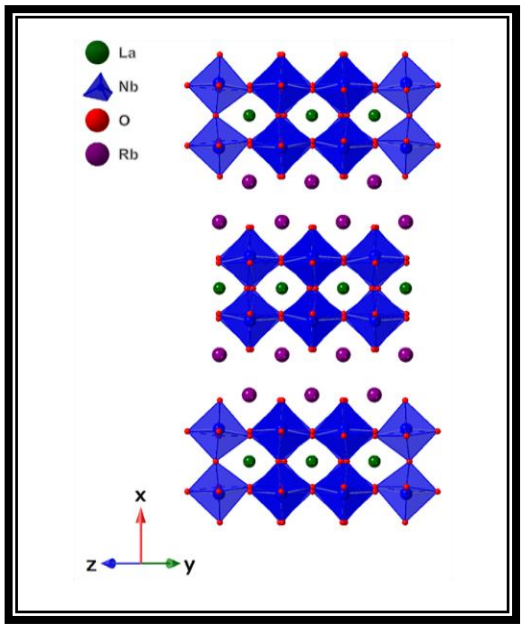

Figure 4. Structure of $Rb_2LaNb_2O_7$. The octahedra represent NbO_6 and Nb-O bonds are shown. Green spheres represent La and purple spheres represent Rb.

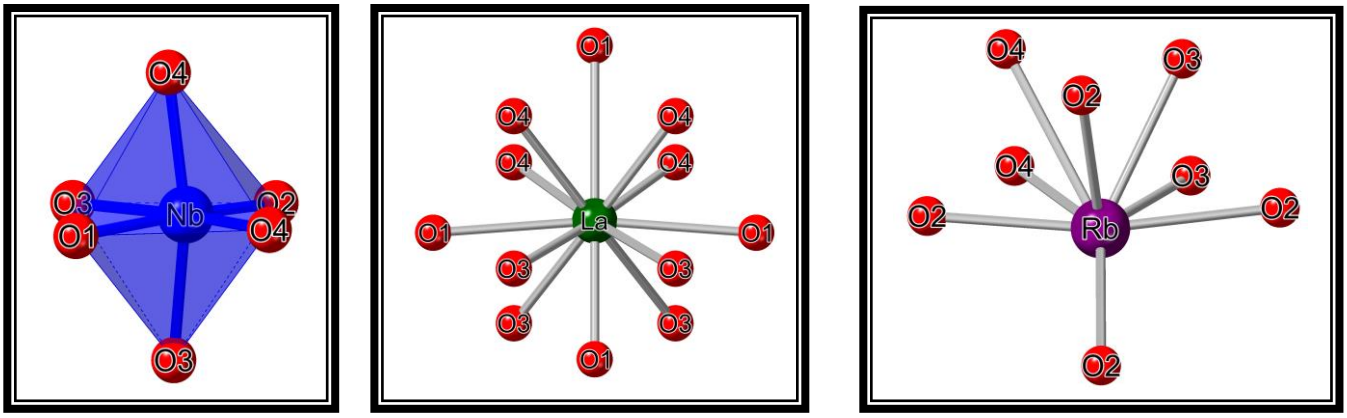

Figure 5. The niobium cation resides in a NbO_6 environment (left). The Lanthanum cation resides in a LaO_{12} environment (middle). The rubidium cation resides in a RbO_8 environment (right).

The niobium atoms in this compound are coordinated to six oxygens to form distorted octahedra. As shown in Table 6, Nb adopts bond distances normally observed in the Nb^{5+}. The Nb-O bond distances range from 1.842 Å to 2.011 Å and the average Nb-O distances in NbO_6 is 2.02 Å. This significantly agrees with the value, 1.99 Å obtained using the sum of the Shannon crystal radii[45,46] for six coordinated Nb^{5+} (0.78 Å) and two-coordinated O^{2-} (1.21Å). In order to provide additional proof for this point and to eliminate the possibility of the occurrence of a Nb^{4+} ion, the BVS calculation was performed with the Nb-O bond lengths obtained from the Crystalmaker structure. Moreover, the previously reported R_0 values extracted from literature for Nb^{4+} and Nb^{5+} that is 1.88 and 1.911, respectively, and *b* was set equal to 0.37 were applied.[2,5] Calculation of the valence for the Nb-O bonds were carried in similar steps to the calculations previously stated for the Nb-O bonds in $RbLaNb_2O_7$. The sum of the valences of the bonds around the Nb ion provide an estimation of its oxidation state. The result of the BVS calculations for Nb is summarized in Table 6. The sum of bond valences is 4.61 v.u. for Nb^{5+} and 4.25 v.u. for Nb^{4+}.

These values indicate a mixed valence for Nb. Thus, it is reasonable to assign that the Nb ion can be in +5 oxidation state and +4 oxidation state.

Table 6. Selected Bond Distances (Å) in NbO_6 octahedra, and Bond valence sum

Bond	**Bond length (Å)**	**Valence**	
		Nb^{4+}	**Nb^{5+}**
Nb-O(1)	2.110	0.54	0.58
Nb-O(2)	1.842	1.11	1.21
Nb-O(3) × 2	2.029	1.34	1.46
Nb-O(4) × 2	2.053	1.26	1.36
	Sum	4.25	4.61

The lanthanum atoms in this compound are coordinated to twelve oxygens to form distorted polyhedra. As shown in Table 7, La adopts bond distances normally observed in the La^{3+}. The La-O bond distances range from 2.515 Å to 3.182Å and the average La-O distances in LaO_{12} is 2.75 Å. This value is significantly close compared to the value of 2.71 Å obtained from the sum of the Shannon crystal radii[45,46] for twelve coordinated La^{3+} (1.50 Å) and two-coordinated O^{2-} (1.21Å). The BVS calculation was performed with the La-O bond lengths obtained from the Crystalmaker structure. Moreover, the previously reported R_0 values extracted from literature for La^{3+} (i,e., 2.172), and the *b* was set equal to 0.37, were applied.[2,5] The result of the BVS calculations for La is summarized in Table 7, where the sum of bond valences was found to be 2.75 v.u. This value is close to the integer three. Thus, it is reasonable to assign that the La ion is in +3 oxidation state.

Table 7. Selected Bond Distances (Å) in LaO_{12} units, and Bond valence sum		
Bond	**Bond length (Å)**	**Valence** **La^{3+}**
La-O(1)	3.182	0.07
La-O(1)	2.515	0.40
La-O(1) × 2	2.855	0.32
La-O(3) × 4	2.768	0.80
La-O(4) × 4	2.632	1.16
	Sum	2.75

The rubidium atoms in this compound are coordinated to eight oxygens to form distorted polyhedra. As shown in Table 8, Rb adopts bond distances normally observed in the Rb^{+}. The Rb-O bond distances range from 2.826 Å to 3.348Å and the average Rb-O distances in RbO_8 is 3.05 Å. This value is significantly close compared to the value of 2.96 Å obtained by the sum of the Shannon crystal radii[45,46] for twelve coordinated Rb^{1+} (1.75 Å) and two-coordinated O^{2-} (1.21Å). The BVS calculation was performed with the Rb-O bond lengths obtained from the Crystalmaker structure. Moreover, the previously reported R_0 values extracted from literature for Rb^{+} (i.e., 2.263), and *b* was set equal to 0.37, were applied.[2,5] The result of the BVS calculations for Rb is summarized in Table 8, where the sum of bond valences was found to be 1.08 v.u. This value is close to the integer one. Thus, it is reasonable to assign that the Rb ion is in +1 oxidation state.

Table 8. Selected Bond Distances (Å) in RbO_8 units, and Bond valence sum

Bond	**Bond length (Å)**	**Valence** **Rb^+**
Rb-O(2)	2.826	0.22
Rb-O(2)	2.874	0.19
Rb-O(2)	2.915	0.17
Rb-O(2)	2.942	0.16
Rb-O(3) × 2	3.059	0.24
Rb-O(4) × 2	3.348	0.10
	Sum	1.08

The third perovskite oxide studied was $NaLaNb_2O_7$ and structure has been refined by Rietveld method. The refinement has been converged to R_{wp} = 11.46% and R_F = 2.11%. The atomic coordinates and the thermal parameters for $NaLaNb_2O_7$ are listed in Table 9. Rietveld analysis conducted on neutron powder diffraction data shows that this phase crystallizes in a tetragonal space group with *a* = 3.9022(1) Å, and *c* = 21.1826(8); *I4/mmm* (No. 139); *Z* =2. Figure 6 shows the structure of $NaLaNb_2O_7$ where the perovskite layers are staggered.[47]

Table 9. Atomic Coordinates and Equivalent Displacement Parameters for $NaLaNb_2O_7$

Atom	Wyckoff notation	x	y	z	Uiso ($Å^2$)[a]
Na	4d	0.0	0.5	0.25	4.9(14)
La	2a	0.0	0.0	0.0	1.9(2)
Nb	4e	0.0	0.0	0.3934(2)	0.8(1)
O(1)	2b	0.0	0.0	0.5	1.9(13)
O(2)	8g	0.0	0.5	0.0895(10)	2.2(7)
O(3)	4e	0.0	0.0	0.3118(15)	3.7(10)

a Uiso is the isotropic atomic displacement parameters obtained from Rietveld refinement.

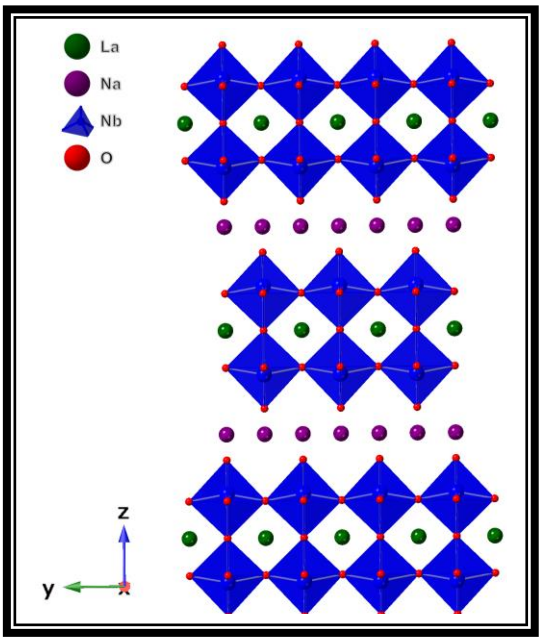

Figure 6. Structure of $NaLaNb_2O_7$. The octahedra represent NbO_6 and Nb-O bonds are shown. The green spheres represent La and the purple spheres represent Na.

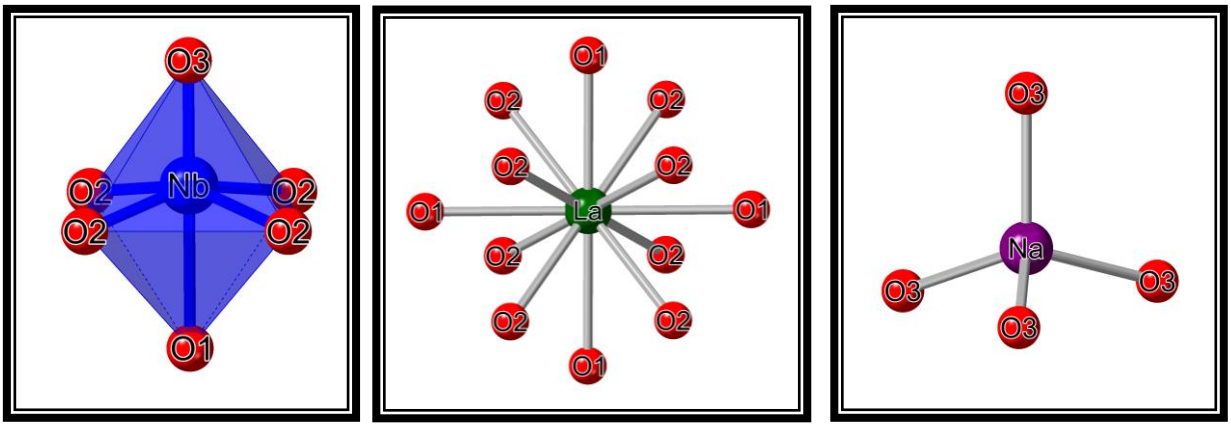

Figure 7. The niobium cation resides in a NbO_6 environment (left). The Lanthanum cation resides in a LaO_{12} environment (middle). The sodium cation adopting a tetrahedral environment (right).

The niobium atoms in this compound are coordinated to six oxygens to form distorted octahedra. As shown in Table 10, Nb adopts bond distances normally observed in the Nb^{5+}. The Nb-O bond distances range from 1.729 Å to 2.258 Å and the average Nb-O distances in NbO_6 is 1.99 Å. This value was found to be the same compared to the average Nb-O bond distances value obtained by the sum of the Shannon crystal radii[45,46] for six coordinated Nb^{5+} (0.78 Å) and two-coordinated O^{2-} (1.21Å). In order to provide additional proof for this point and to eliminate the possibility of the occurrence of a Nb^{4+} ion, the BVS calculation was performed with the Nb-O bond lengths obtained from the Crystalmaker structure. Moreover, the previously reported R_0 values extracted from literature for Nb^{4+} and Nb^{5+} that is 1.88 and 1.911, respectively, and *b* was set equal to 0.37 were applied.[2,5] The result of the BVS calculations for Nb is summarized in Table 10. The sum of bond valences is 5.31 v.u. for Nb^{5+} and 4.88 v.u. for Nb^{4+} and these values are closer to the integer five. Thus, it is reasonable to assign that the Nb ion is in +5 oxidation state.

Table 10. Selected Bond Distances (Å) in NbO_6 octahedra, and Bond valence sum

Bond	**Bond length (Å)**	**Valence**	
		Nb^{4+}	**Nb^{5+}**
Nb-O(1)	2.258	0.36	0.39
Nb-O(2) × 4	1.984	3.04	3.28
Nb-O(3)	1.729	1.50	1.64
	Sum	4.88	5.31

The lanthanum atoms in this compound are coordinated to twelve oxygens to form distorted polyhedra. As shown in Table 11, La adopts bond distances normally observed in the La^{3+}. The La-O bond distances range from 2.721 Å to 2.759 Å and the average La-O distances in LaO_{12} is

2.73 Å. This value is significantly close to the value 2.71 Å obtained using the sum of the Shannon crystal radii[45,46] for twelve coordinated La^{3+} (1.50 Å) and two-coordinated O^{2-} (1.21Å). The BVS calculation was performed with the La-O bond lengths obtained from the Crystalmaker structure. Moreover, the previously reported R_0 values extracted from literature for La^{3+} (i,e., 2.172), and the *b* was set equal to 0.37, were applied.[2,5] The result of the BVS calculations for La is summarized in Table 11, where the sum of bond valences was found to be 2.64 v.u. This value is close to the integer three. Usually, the bond valence sum contains variations of about 10% even in typical compounds, which could be attributed to accuracy of the interatomic distances and feature of the empirical formula. Thus, it is reasonable to assign that the La ion is in +3 oxidation state.

Table 11. Selected Bond Distances (Å) in LaO_{12} units, and Bond valence sum

Bond	**Bond length (Å)**	**Valence** La^{3+}
La-O(1) × 4	2.759	0.80
La-O(2) × 8	2.721	1.84
	Sum	2.64

The sodium atoms in this compound are coordinated to four oxygens to form a tetrahedra. As shown in Table 12, Na atoms adopt bond distances normally observed in the Na^{1+}. The Na-O bond distances were equal to 2.350 Å and the average Na-O distances in NaO_4 is 2.35 Å. This comparable with 2.34 Å, the sum of the Shannon crystal radii[45,46] for four coordinated Na^{1+} (1.13 Å) and two-coordinated O^{2-} (1.21Å). The BVS calculation was performed with the Na-O bond lengths obtained from the Crystalmaker structure. Moreover, the previously reported R_0 values extracted from literature for Na^{1+} that is 1.803 and *b* was set equal to 0.37 were applied.[2,5] The

result of the BVS calculations for Na is summarized in Table 12, where the sum of bond valences was found to be 0.92 v.u. This value is close to the integer one. Thus, it is reasonable to assign that the Na ion is in +1 oxidation state.

Table 12. Selected Bond Distances (Å) in NaO_4 units, and Bond valence sum

Bond	**Bond length (Å)**	**Valence** Na^{1+}
Na-O(3) × 4	2.350	0.92
	Sum	0.92

The fourth perovskite oxide studied was $(Cs_2Cl)LaNb_2O_7$ and structure has been refined by Rietveld method. The refinement has been converged to a factor χ^2 =2.06. The atomic coordinates and the thermal parameters for $(Cs_2Cl)LaNb_2O_7$ are listed in Table 13. Rietveld analysis conducted on powder diffraction data shows that this phase crystallizes in a tetragonal space group with *a* = 3.92182(1) Å, and *c* = 15.3107(3); *P4/mmm* (No. 123); *Z* = 1. Figure 8 shows the structure of $(Cs_2Cl)LaNb_2O_7$.[48]

Table 13. Atomic Coordinates and Equivalent Displacement Parameters for $(Cs_2Cl)LaNb_2O_7$

Atom	Wyckoff notation	x	y	z	Uiso ($Å^2$)[a]
Cs	2g	0	0	0.3609(1)	1.5(1)
Cl	1d	0.5	0.5	0.5	1.3(3)
La	1a	0	0	0	1.09(1)
Nb	2h	0.5	0.5	0.1460(2)	0.4(1)
O(1)	2h	0.5	0.5	0.2564(9)	2.7(5)
O(2)	1c	0.5	0.5	0	2.0
O(3)	4i	0	0.5	0.1231(6)	2.9(3)

a Uiso is the isotropic atomic displacement parameters obtained from Rietveld refinement.

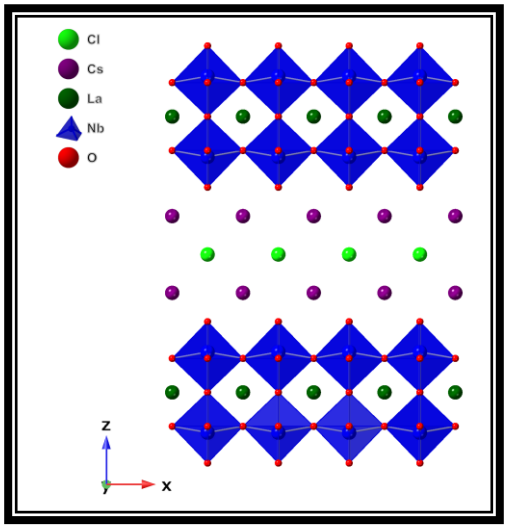

Figure 8. Structure of $(Cs_2Cl)LaNb_2O_7$. The octahedra represent NbO_6 and Nb-O bonds are shown. Green spheres represent La, neon green spheres represent Cl, and purple spheres represent Cs.

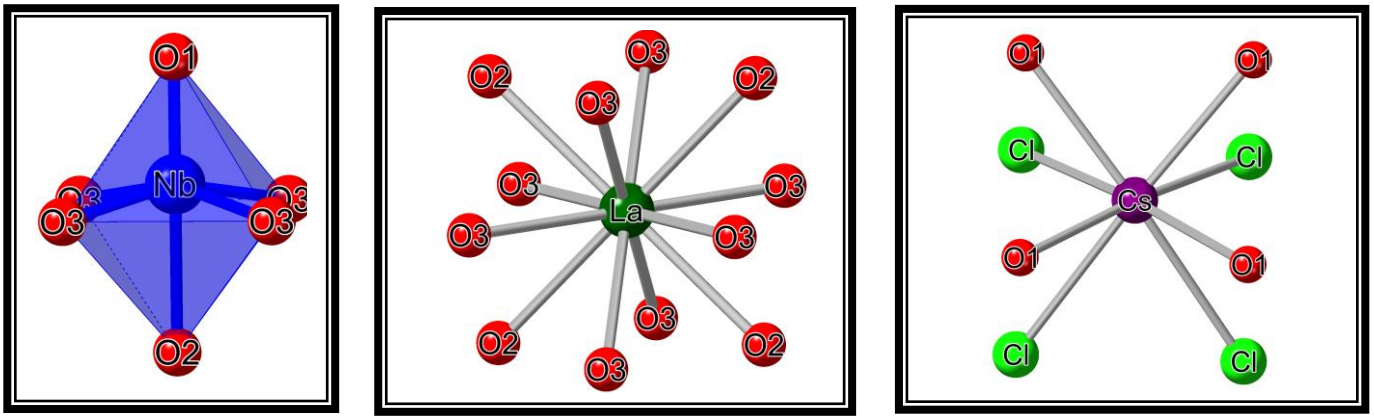

Figure 9. The niobium cation resides in a NbO_6 environment (left). The Lanthanum cation resides in a LaO_{12} environment (middle). The cesium cation resides in a $CsCl_4O_4$ environment (right).

The niobium atoms in this compound are coordinated to six oxygens to form distorted octahedra. As shown in Table 14, Nb adopts bond distances normally observed in the Nb^{5+}. The Nb-O bond distances range from 1.690 Å to 2.235 Å and the average Nb-O distances in NbO_6 is 1.99 Å. This value was found to be the same compared to the average Nb-O bond distances value obtained by the sum of the Shannon crystal radii[45,46] for six coordinated Nb^{5+} (0.78 Å) and two-

coordinated O^{2-} (1.21Å). In order to provide additional proof for this point and to eliminate the possibility of the occurrence of a Nb^{4+} ion, the BVS calculation was performed with the Nb-O bond lengths obtained from the Crystalmaker structure. Moreover, the previously reported R_0 values extracted from literature for Nb^{4+} and Nb^{5+} that is 1.88 and 1.911, respectively, and *b* was set equal to 0.37 were applied.[2,5] The result of the BVS calculations for Nb is summarized in Table 14. The sum of bond valences is 5.44 v.u. for Nb^{5+} and 5.01 v.u. for Nb^{4+} and these values are closer to the integer five. Thus, it is reasonable to assign that the Nb ion is in +5 oxidation state.

Table 14. Selected Bond Distances (Å) in NbO_6 octahedra, and Bond valence sum

Bond	**Bond length (Å)**	**Valence**	
		Nb^{4+}	**Nb^{5+}**
Nb-O(1)	1.690	1.67	1.82
Nb-O(2)	2.235	0.38	0.42
Nb-O(3) × 4	1.992	2.96	3.20
	Sum	5.01	5.44

The lanthanum atoms in this compound are coordinated to twelve oxygens to form distorted polyhedra. As shown in Table 15, La adopts bond distances normally observed in the La^{3+}. The La-O bond distances range from 2.720 Å to 2.773Å and the average La-O distances in LaO_{12} is 2.74 Å. This comparable with 2.71 Å, the sum of the Shannon crystal radii[45,46] for twelve coordinated La^{3+} (1.50 Å) and two-coordinated O^{2-} (1.21Å). The BVS calculation was performed with the La-O bond lengths obtained from the Crystalmaker structure. Moreover, the previously reported R_0 values extracted from literature for La^{3+} (i,e., 2.172), and the *b* was set equal to 0.37, were applied.[2,5] The result of the BVS calculations for La is summarized in Table 15, where the

sum of bond valences was found to be 2.64 v.u. This value is close to the integer three. Thus, it is reasonable to assign that the La ion is in +3 oxidation state.

Table 15. Selected Bond Distances (Å) in LaO_{12} units, and Bond valence sum

Bond	**Bond length (Å)**	**Valence** La^{3+}
La-O(2) × 4	2.773	0.80
La-O(3) × 8	2.720	1.84
	Sum	2.64

The cesium atoms in this compound are coordinated to four oxygens and four chlorines to form distorted cuboid. As shown in Table 16, Cs atoms adopt bond distances normally observed in the Cs^{1+}. The Cs-O and Cs-Cl bond distances were equal to 3.202 Å and 3.497 Å, respectively. The average Cs-O distances in CsO_4 is 3.20, this comparable with 3.09 Å, the sum of the Shannon crystal radii[45,46] for eight coordinated Cs^{1+} (1.88 Å) and two-coordinated O^{2-} (1.21Å). The average Cs-Cl distances in $CsCl_4$ is 3.50 Å, which is significantly close compared with 3.55 Å, obtained from the sum of the Shannon crystal radii[45,46] for eight coordinated Cs^{1+} (1.88 Å) and two-coordinated Cl^- (1.67Å). The BVS calculation was performed with Cs-Cl and Cs-O) bonds obtained from the Crystalmaker structure. Moreover, the previously reported R_0 value for Cs^{1+} bonded to O or Cl (i.e., 2.417 and 2.79, respectively), and *b* was set equal to 0.37, were applied.[2,5] The result of the BVS calculations for Cs is summarized in Table 16, where the sum of bond valences was found to be 1.08 v.u. This value is close to the integer one. Thus, it is reasonable to assign that the Cs ion is in +1 oxidation state.

Table 16. Selected Bond Distances (Å) in $CsCl_4O_4$ units, and Bond valence sum		
Bond	**Bond length (Å)**	**Valence** Cs^{1+}
Cs-O(1) × 4	3.202	0.48
Cs-Cl × 4	3.497	0.60
	Sum	1.08

The fifth perovskite oxide studied was $(FeCl)LaNb_2O_7$ and structure has been refined by Rietveld method. The refinement has been converged to a factor of χ^2 =1.612. The atomic coordinates and the thermal parameters for $(FeCl)LaNb_2O_7$ are listed in Table 17. Rietveld analysis conducted on neutron powder diffraction data shows that this phase crystallizes in a tetragonal space group with *a* = 3.879(1) Å, and *c* = 11.861(5); *P4/mmm* (No. 123); *Z* = 1. Figure 10 shows the structure of $(FeCl)LaNb_2O_7$ where the perovskite layers are eclipsed, and the lower layer charge allows the Rb^+ to reside in a cubic site extended away from the perovskite block.[49]

Table 17. Atomic Coordinates and Equivalent Displacement Parameters for $(FeCl)LaNb_2O_7$

Atom	Wyckoff notation	x	y	z	Uiso ($Å^2$)[a]
Fe	4o	0.421(2)	0.5	0.5	0.007(2)
Cl	1b	0	0	0.5	0.038(2)
La	1a	0	0	0	0.0137(4)
Nb	2h	0.5	0.5	0.19057(6)	0.0133(4)
O(1)	4i	0	0.5	0.1546(3)	0.018(1)
O(2)	2h	0.5	0.5	0.3358(5)	0.024(2)
O(3)	1c	0.5	0.5	0	0.016(3)

a Uiso is the isotropic atomic displacement parameters obtained from Rietveld refinement.

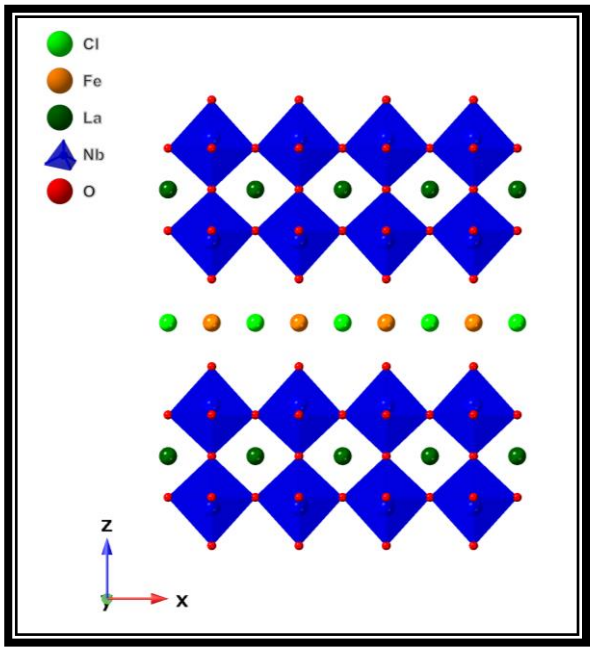

Figure 10. Structure of (FeCl)$LaNb_2O_7$. The octahedra represent NbO_6 and Nb-O bonds are shown. Green spheres represent La, orange spheres represent Fe, and neon green spheres represent Cl.

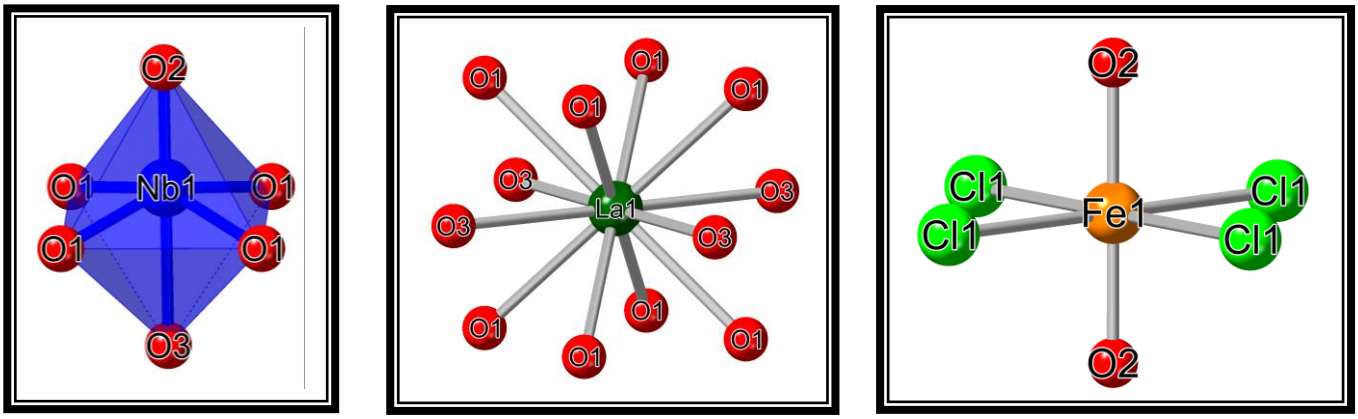

Figure 11. The niobium cation resides in a NbO_6 environment (left). The Lanthanum cation resides in a LaO_{12} environment (middle). The iron cation resides in a $FeCl_4O_2$ environment (right).

The niobium atoms in this compound are coordinated to six oxygens to form distorted octahedra. As shown in Table 18, Nb adopts bond distances normally observed in the Nb^{5+}. The Nb-O bond distances range from 1.723 Å to 2.260 Å and the average Nb-O distances in NbO_6 is 1.99 Å. This value was found to be the same compared to the average Nb-O bond distances value

obtained by the sum of the Shannon crystal radii[45,46] for six coordinated Nb^{5+} (0.78 Å) and two-coordinated O^{2-} (1.21Å). In order to provide additional proof for this point and to eliminate the possibility of the occurrence of a Nb^{4+} ion, the BVS calculation was performed with the Nb-O bond lengths obtained from the Crystalmaker structure. Moreover, the previously reported R_0 values extracted from literature for Nb^{4+} and Nb^{5+} that is 1.88 and 1.911, respectively, and *b* was set equal to 0.37 were applied.[2,5] The sum of the valences of the bonds around the Nb ion provide an estimation of its oxidation state. The result of the BVS calculations for Nb is summarized in Table 18. The sum of bond valences is 5.33 v.u. for Nb^{5+} and 4.89 v.u. for Nb^{4+} and these values are closer to the integer five. Thus, it is reasonable to assign that the Nb ion is in +5 oxidation state.

Table 18. Selected Bond Distances (Å) in NbO_6 octahedra, and Bond valence sum

Bond	**Bond length (Å)**	**Valence**	
		Nb^{4+}	**Nb^{5+}**
Nb-O(1) × 4	1.986	3.00	3.28
Nb-O(2)	1.723	1.53	1.66
Nb-O(3)	2.260	0.36	0.39
	Sum	4.89	5.33

The lanthanum atoms in this compound are coordinated to twelve oxygens to form distorted polyhedra. As shown in Table 19, La adopts bond distances normally observed in the La^{3+}. The La-O bond distances range from 2.669 Å to 2.743 Å and the average La-O distances in LaO_{12} is 2.69 Å. Significantly close compared with 2.71 Å, the sum of the Shannon crystal radii[45,46] for twelve coordinated La^{3+} (1.50 Å) and two-coordinated O^{2-} (1.21Å). The BVS calculation was performed with the La-O bond lengths obtained from the Crystalmaker structure. Moreover, the

previously reported R_0 values extracted from literature for La^{3+} (i,e., 2.172), and the *b* was set equal to 0.37, were applied.[2,5] The result of the BVS calculations for La is summarized in Table 19, where the sum of bond valences was found to be 2.92 v.u. This value is close to the integer three. Thus, it is reasonable to assign that the La ion is in +3 oxidation state.

Table 19. Selected Bond Distances (Å) in LaO_{12} units, and Bond valence sum

Bond	**Bond length (Å)**	**Valence** **La^{3+}**
La-O(1) × 8	2.669	2.08
La-O(3) × 4	2.743	0.84
	Sum	2.92

The iron atoms in this compound are coordinated to two oxygens and four chlorines to form distorted octahedra. As shown in Table 20, Fe adopts bond distances normally observed in the Fe^{2+}. The Fe-O bond distances were equal to 1.948 Å, while the Fe-Cl bond distances were equal to 2.743 Å. The average Fe-O distances in FeO_4 is 1.95 Å. This is significantly close compared with 1.98 Å, the sum of the Shannon crystal radii[45,46] for six coordinated Fe^{2+} (0.77 Å) and two-coordinated O^{2-} (1.21Å). The average Fe-Cl distances in $FeCl_4$ is 2.74 Å. This comparable with 2.44 Å, the sum of the Shannon crystal radii[45,46] for six coordinated Fe^{2+} (0.77 Å) and four-coordinated Cl^- (1.67Å).

In order to provide additional proof for this point and to eliminate the possibility of the occurrence of a Fe^{2+} ion, the BVS calculation was performed with the Fe-O and Fe-Cl bond lengths obtained from the Crystalmaker structure. Moreover, the previously reported R_0 values Fe^{2+} and Fe^{3+} (i.e., 1.734 and 1.759, respectively when bonded to O^{-2}, and 2.06 and 2.09, respectively when

bonded to Cl^-), and *b* was set equal to 0.37, were applied.[2,5] The result of the BVS calculations for Fe is summarized in Table 20. The sum of bond valences is 1.76 v.u. for Fe^{2+} and 1.89 v.u. for Fe^{3+} and these values are closer to the integer two. Thus, it is reasonable to assign that the Fe ion is in +2 oxidation state.

Table 20. Selected Bond Distances (Å) in $FeCl_4O_2$ units, and Bond valence sum

Bond	**Bond length (Å)**	**Valence**	
		Fe^{2+}	**Fe^{3+}**
Fe-O(2) × 2	1.948	1.12	1.20
Fe-Cl(1) × 4	2.743	0.64	0.68
	Sum	1.76	1.88

The sixth perovskite oxide studied was $Rb_2S_xLaNb_2O_7$ (~ $x \leq 0.8$), and structure has been refined by Rietveld method. The refinement has been converged to a factor of χ^2 =2.07. The atomic coordinates and the thermal parameters for $Rb2S_xLaNb_2O_7$ are listed in Table 21. Rietveld analysis conducted on powder diffraction data shows that this phase crystallizes in a tetragonal space group with *a* = 3.8998(2) Å, and *c* = 15.255(1); *P4/mmm* (No. 123); *Z* = 1. Figure 12 shows the structure of $Rb_2S_xLaNb_2O_7$ ($x \leq 0.8$) where the perovskite layers are eclipsed, and the lower layer charge allows the Rb^+ to reside in a cubic site extended away from the perovskite block.[50]

Table 21. Atomic Coordinates and Equivalent Displacement Parameters for $Rb_2S_xLaNb_2O_7$

Atom	Wyckoff notation	x	y	z	g	Uiso ($Å^2$)[a]
Nb	2h	0.5	0.5	0.1480(2)	1.06(2)	0.005
La	1a	0	0	0	0.76(3)	0.002(1)
Rb	2g	0	0	0.3488(3)	1	0.041(2)
S	1d	0.5	0.5	0.5	1	0.014
O(1)	2h	0.5	0.5	0.267(2)	1	0.03(1)
O(2)	1c	0.5	0.5	0	1	0.03(1)
O(3)	4i	0	0.5	0.127(1)	1	0.016(5)

a Uiso is the isotropic atomic displacement parameters obtained from Rietveld refinement.

g = occupation factor

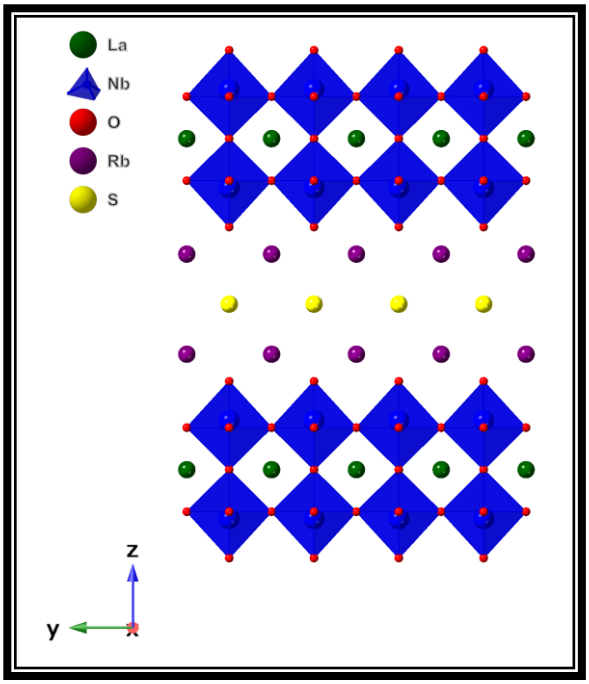

Figure 12. Structure of $Rb_2S_xLaNb_2O_7$ (~ $x \leq 0.8$). The octahedra represent NbO_6 and Nb-O bonds are shown. Green spheres represent La, yellow spheres represent sulfur, and purple spheres represent Rb.

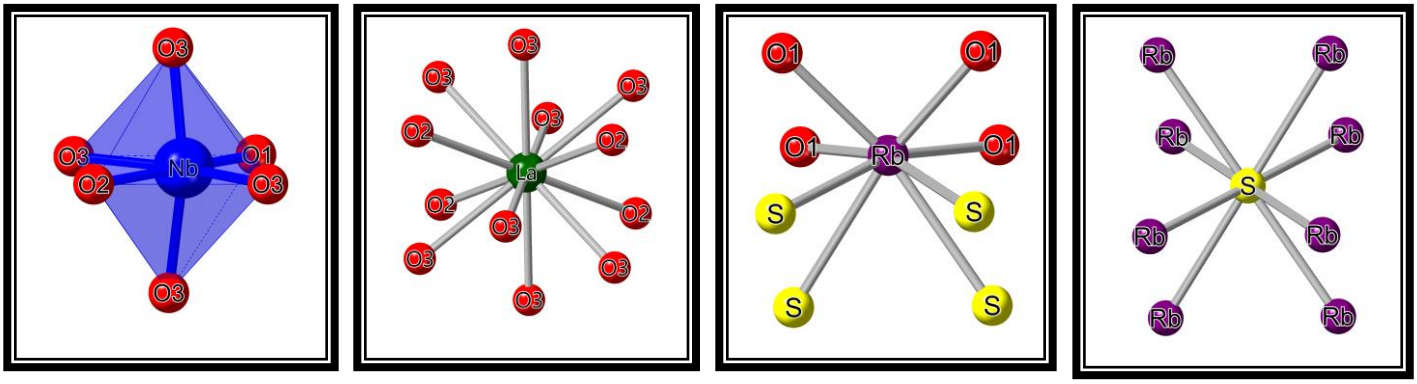

Figure 13. From left to right, the niobium cation resides in a NbO_6 environment, the lanthanum cation resides in a LaO_{12} environment, the rubidium cation resides in a RbS_4O_4 environment, and the sulfur anion resides in cuboid environment.

The niobium atoms in this compound are coordinated to six oxygens to form distorted octahedra. As shown in Table 22, Nb adopt bond distances normally observed in the Nb^{5+}. The Nb-O bond distances range from 1.815 Å to 2.258 Å and the average Nb-O distances in NbO_6 is 2.00 Å. Significantly close compared with 1.99 Å, the sum of the Shannon crystal radii[45,46] for six coordinated Nb^{5+} (0.78 Å) and two-coordinated O^{2-} (1.21Å). In order to provide additional proof for this point and to eliminate the possibility of the occurrence of a Nb^{4+} ion, the BVS calculation was performed with the Nb-O bond lengths obtained from the Crystalmaker structure. Moreover, the previously reported R_0 values extracted from literature for Nb^{4+} and Nb^{5+} that is 1.88 and 1.911, respectively, and b was set equal to 0.37 were applied.[2,5]

The sum of the valences of the bonds around the Nb ion provide an estimation of its oxidation state. The result of the BVS calculations for Nb is summarized in Table 22. The sum of bond valences is 5.05 v.u. for Nb^{5+} and 4.63 v.u. for Nb^{4+} and these values are closer to the integer five. Thus, it is reasonable to assign that the Nb ion is in +5 oxidation state.

Table 22. Selected Bond Distances (Å) in NbO_6 octahedra, and Bond valence sum			
Bond	**Bond length (Å)**	**Valence**	
		Nb^{4+}	**Nb^{5+}**
Nb-O(1)	1.815	1.19	1.30
Nb-O(2)	2.258	0.36	0.39
Nb-O(3) × 4	1.976	3.08	3.36
	Sum	4.63	5.05

The lanthanum atoms in this compound are coordinated to twelve oxygens to form distorted polyhedra. As shown in Table 23 La adopts bond distances normally observed in the La^{3+}. The La-O bond distances range from 2.749 Å to 2.758Å and the average La-O distances in LaO_{12} is 2.75 Å. This comparable with 2.71 Å, the sum of the Shannon crystal radii[45,46] for twelve coordinated La^{3+} (1.50 Å) and two-coordinated O^{2-} (1.21Å). The BVS calculation was performed with the La-O bond lengths obtained from the Crystalmaker structure. Moreover, the previously reported R_0 values extracted from literature for La^{3+} (i,e., 2.172), and the *b* was set equal to 0.37, were applied.[2,5] The result of the BVS calculations for La is summarized in Table 23, where the sum of bond valences was found to be 2.52 v.u. This value is close to the integer three. Thus, it is reasonable to assign that the La ion is in +3 oxidation state.

Table 23. Selected Bond Distances (Å) in LaO_{12} units, and Bond valence sum		
Bond	**Bond length (Å)**	**Valence** **La^{3+}**
La-O(3) × 8	2.749	1.68
La-O(2) × 4	2.758	0.84
	Sum	2.52

The rubidium atoms in this compound are coordinated to four oxygens and four sulfurs to form distorted cuboid. As shown in Table 24, Rb adopts bond distances normally observed in the Rb^{+}. The Rb-O bond distances are equal to 3.027 Å, while the Rb-S bond distances are equal to 3.959Å. The average Rb-O(1) distances is 3.03 Å. Significantly close compared with 2.96 Å, the sum of the Shannon crystal radii[45,46] for eight coordinated Rb^{1+} (1.75 Å) and two-coordinated O^{2-} (1.21Å). The average Rb-S distances calculated is 3.60 Å. Slightly higher than 3.45 Å, the sum of the Shannon crystal radii[45,46] for eight coordinated Rb^{+} (1.75 Å) and four-coordinated S^{2-} (1.70Å). The result of the BVS calculations for Rb is summarized in Table 24, where the sum of bond valences was found to be 0.88 v.u. This value is close to the integer one. Thus, it is reasonable to assign that the Rb ion is in +1 oxidation state.

Table 24. Selected Bond Distances (Å) in RbS_4O_4 units, and Bond valence sum

Bond	**Bond length (Å)**	**Valence** **Rb^{+}**
Rb-O(1) × 4	3.027	0.52
Rb-S × 4	3.595	0.36
	Sum	0.88

The Bond-valence summations for each anion were calculated for both anionic sites from relevant bond distances. The final values resulted from BVS calculations for the oxygens can be summarized as 1.80, 1.60, and 2.10 valence units for O(1), O(2), and O(3), respectively, which in each case is close to the expected values of 2 for oxygen. Furthermore, the BVS for eight coordinated sulfur atoms with rubidium atoms was calculated and the result was summarized in

Table 25, where the sum of bond valences was found to be 0.71 v.u. Hence, it can be said that the sulfur bond valence sum diverges significantly from integer two. The average Rb-S distances calculated is 3.60 Å and this is slightly higher than 3.45 Å, the sum of the Shannon crystal radii[45,46]. Usually, an increase of bond distance between cation and anions could result in deviation of the bond valences considerably but this argument is not valid for this particular case.

Table 25. Selected Bond Distances (Å) in SRb_8 units, and Bond valence sum

Bond	**Bond length (Å)**	**Valence** S^{2-}
Rb-S× 8	3.595	0.71
	Sum	0.71

As shown in Table 26, the total number of Rb, La, Nb, O, and S atoms belonging to the unit cell can be calculated and the ratio of Rb : La : Nb : O : S is 3:1:2:7:1. Based on this ratio, the overall formula can be formulated as $Rb_2SLaNb_2O_7$. However, the charges are not balanced as there is an additional -1 charge if the oxidation of sulfur is considered to be -2 (i.e., S^{2-}). If S^{2-} content were 0.5 (i.e., $Rb_2S_{0.5}LaNb_2O_7$), then the compound would have ideal charged balance formula. The reported sulfur composition obtained in the Rietveld refinement, ca. ~0.8 (Table 21), is greater than 0.5.[50]

Furthermore, to validate this sulfur composition, the authors have suggested that the high sulfur content is due to the presence of HS^- and this argument has been supported by Raman spectroscopy (i.e., H-S stretch in the range 2500-2600 cm^{-1}).[50] The BVS value calculated for sulfur (0.71 v.u.) shows that the BVS method is surprisingly accurate to estimate oxidation state for sulfur

in this compound. The oxidation state of the sulfur is obviously lower than the expected value because the contributions from hydrogen atoms could not be incorporated to our calculations.

Table 26: Number of atoms per unit cell in $Rb_2S_xLaNb_2O_7$

Site	Rb	La	Nb	O	S
Central	0	0	2	2	1
Face	0	0	0	10 ×½ =5	0
Edge	8× ¼= 2	0	0	0	0
Corner	0	8× (1/8) = 1	0	0	0
Total	2	1	2	7	1

The final calculated BVS values for metal ions Nb, La, Rb, Na, Cs, Fe, and S of the six layered perovskite compounds including, $RbLaNb_2O_7$, $Rb_2LaNb_2O_7$, $Rb_2S_xLaNb_2O_7$ ($\sim x \leq 0.8$), $NaLaNb_2O_7$, $(Cs_2Cl)LaNb_2O_7$, and $(FeCl)LaNb_2O_7$, are all summarized and given in Table 27.

Table 27. The summary of the bond valence sum				
Atom	**Coordination Number**	**Oxidation Number**	**Metal Ion**	**BVS**
Rubidium Ion				
Rb in $RbLaNb_2O_7$	8	1	Rb^{+}	0.85
Rb in $Rb_2LaNb_2O_7$	8	1	Rb^{+}	1.08
Rb in $Rb_2S_xLaNb_2O_7$	8	1	Rb^{+}	0.88
Niobium Ion				
Nb in $RbLaNb_2O_7$	6	5	Nb^{4+}	4.72
			Nb^{5+}	5.12
Nb in $Rb_2LaNb_2O_7$	6	5 and 4	Nb^{4+}	4.25
			Nb^{5+}	4.61
Nb in $Rb_2S_xLaNb_2O_7$	6	5	Nb^{4+}	4.63
			Nb^{5+}	5.05
Nb in $NaLaNb_2O_7$	6	5	Nb^{4+}	4.88
			Nb^{5+}	5.31
Nb in $(Cs_2Cl)LaNb_2O_7$	6	5	Nb^{4+}	5.01
			Nb^{5+}	5.44
Nb in $(FeCl)LaNb_2O_7$	6	5	Nb^{4+}	4.89
			Nb^{5+}	5.33
Lanthnum Ion				
La in $RbLaNb_2O_7$	12	3	La^{3+}	2.98
La in $Rb_2LaNb_2O_7$	12	3	La^{3+}	2.75
La in $Rb_2S_xLaNb_2O_7$	12	3	La^{3+}	2.52
La in $NaLaNb_2O_7$	12	3	La^{3+}	2.64
La in $(Cs_2Cl)LaNb_2O_7$	12	3	La^{3+}	2.61
La in $(FeCl)LaNb_2O_7$	12	3	La^{3+}	2.92
Sodium, Cesium, Iron, and Sulfur				
Na in $NaLaNb_2O_7$	4	1	Na^{1+}	0.92
Cs in $(Cs_2Cl)LaNb_2O_7$	8	1	Cs^{1+}	1.08
Fe in $(FeCl)LaNb_2O_7$	6	2	Fe^{2+}	1.76
			Fe^{3+}	1.88
S in $Rb_2S_xLaNb_2O_7$	8	-1/-2	S^{-}/S^{2-}	0.71

As previously stated, the Rietveld refinement result may be the best that can be done and may be of great value for crystal structure determination. However, further inspection is needed to understand the discrepancies so that one can explore whether the determination of oxidation state

using the bond distances derived from the Rietveld refinement method could be used as an alternative measure of refinement quality along with the reported χ^2 values (and other *R* factors). In general, the values of Rietveld profile parameter such as R_F, R_{wp}, R_E and χ^2 are less than 10% in that way it indicates the goodness of Rietveld analysis.[39] The good agreement with expected oxidations of elements in all the structures analyzed (Table 27) and the reported Rietveld discrepancy values (Table 28), suggest that these two factors are correlated to test the validity of the structure solution.

Table 28: Rietveld reported discrepancy values, (i.e., R_{wp} , R_E, and χ^2)

Compound	
$RbLaNb_2O_7$	R_{wp}=6.9%, R_E=5.2%
$Rb_2LaNb_2O_7$	R_{wp}=3.9%, R_E=1.2%
$Rb_2S_xLaNb_2O_7$	χ^2=2.07
$(Cs_2Cl)LaNb_2O_7$	χ^2=2.06
$(FeCl)LaNb_2O_7$	χ^2=1.61
$NaLaNb_2O_7$	R_{wp}=11.46%, R_F=2.11%

Conclusion

The overall purpose of this study is to explore whether the determination of oxidation state using the bond distances derived from the Rietveld refinement method could be used as an alternative measure of refinement quality along with the reported χ^2 values in the published structure. Good agreement between the calculated and the expected oxidation states would provide support for the chemical formula and the accuracy of a crystal structure determination achieved by Rietveld analysis. To assign the oxidation state using the bond distances, the BVS model was applied by comparing atom valences to the sums of their experimental bond valences. Moreover, the oxidation states of metal ions, niobium, lanthanum, and rubidium were calculated using the crystallographic data of six layered perovskite compounds including, $RbLaNb_2O_7$, $Rb_2LaNb_2O_7$, $Rb_2S_xLaNb_2O_7$ ($x \leq 0.8$), $NaLaNb_2O_7$, $(Cs_2Cl)LaNb_2O_7$, and $(FeCl)LaNb_2O_7$. Additionally, the

oxidation state of metal ions sodium, cesium, and iron were also calculated using the crystallographic data of the layered perovskite $NaLaNb_2O_7$, $(Cs_2Cl)LaNb_2O_7$, and $(FeCl)LaNb_2O_7$, respectively. Starting with the niobium metal ion (Nb) in a NbO_6 octahedra, it was found that the resulted BVS for Nb in $RbLaNb_2O_7$, $Rb_2S_xLaNb_2O_7$ ($x \leq 0.8$), $NaLaNb_2O_7$, $(FeCl)LaNb_2O_7$, and $(Cs_2Cl)LaNb_2O_7$ have shown that Nb atoms adopt a penta-valence state (Nb^{5+}). On the other hand, the Nb atoms in the $Rb_2LaNb_2O_7$ compound, adopt a mixed valance state (i.e., Nb^{4+} and Nb^{5+}) to balance the overall charge of these two compounds.

Furthermore, the resulted BVS for lanthanum atoms (La) in LaO_{12} polyhedra, adopt a tri-valence state (La^{3+}) for all compounds except in $Rb_2S_xLaNb_2O_7$, $NaLaNb_2O_7$, $(Cs_2Cl)LaNb_2O_7$. For these three compounds, the calculated BVS of La atoms reported were (2.52, 2.64, and 2.61) v.u., respectively. These values had significantly deviated from the expected oxidation state value for a La anion (i.e., +3 oxidation state). Additionally, the BVS results shows a good agreement for the oxidation states of rubidium, cesium, and sodium atoms adopting a mono-valence state, that is Rb^{1+}, Cs^{1+}, and Na^{1+}, respectively. While a good agreement for the oxidation state of the iron atoms adopts a di-valent state, Fe^{2+}, to balance the overall charge of the $(FeCl)LaNb_2O_7$ compound.

In conclusion, the determination of oxidation state using the bond distances derived from the Rietveld refinement method for metal ions, niobium, lanthanum, rubidium, sodium, cesium, and iron were in good agreement with the expected oxidation states, (Nb^{4+} and Nb^{5+}), La^{3+}, Rb^{1+}, Na^{1+}, Cs^{1+}, and Fe^{2+}, respectively. Moreover, reviewing the reported χ^2 values (and other *R* factors), in the published structure of the six-compound studied here, have also suggested that the model produces better agreement with the Rietveld data. Hence, Coordination chemists should be able to apply the BVS method as an alternative analysis tool measuring the refinement quality. In

which, it enables them to validate the results of a crystal structure determination, or oxidation states assignment.

References

1. Housecroft C, Sharpe A.G. *Inorg. Chem.*, 4th Ed.: Pearson Education: Essex, **2012**.
2. Brese, N. E.; O'Keefe, M. *Acta Crystallogr*. **1991**, B47, 192-197.
3. Brown, I.D. *Chem. Rev*. **2009**, *109*, 6858–6919.
4. Pauling, L. *J. Am. Chem. Soc*. **1929**, *51*, 1010-1026.
5. Brown, I. D.; Altermatt, D. *Acta. Crystallogr*. **1985**, *B41*, 244-247.
6. Bragg, W. L. Z. *Kristallogr*. **1930**, *74*, 237-305.
7. Zheng, H.; Langner, K.M.; Shields, G.P.; Hou, J.; Kowiel, M.; Allen, F.H.; Murshudov, G.; Minor, W. *Acta Crystallogr. Sect. D*. **2017**, *73(4)*, 316–325.
8. Etxebarria, I.; Perez-Mato, J. M.; Garcia, A.; Blaha, P.; Schwarz, K.; RodriguezCarvajal, *J. Phys. Rev. B* **2005**, *72*, 174108-174116.
9. Brown, I. D. *Acta Crystallogr. Sect.B*. **1992**, *B48*, 553-572.
10. O'Keeffe, M. *Acta Crystallogr. Sect. A*. **1990**, *A46*, 138-142.
11. Nguyen, Tu N. *ChemRxiv*. **2020**, 1-10.
12. West, A. R. *Solid State Chemistry and its Applications*; John Wiley & Sons, Ltd.: Chichester, West Sussex, **2014**; 54–57.
13. D. Montasserasadi, "New Dion-Jacobson and Ruddlesden- Popper Layered Perovskites prepared by Topochemical Methods". University of New Orleans Theses and Dissertations. **2015**. https://scholarworks.uno.edu/td/1985.
14. Ranmohotti, K. G. S.; Josepha E. A.; Choi J.; Zhang J.; Wiley J. B. *Adv. Mater*. **2011**, *23*, 442–460.
15. Palmer, D. C. CrystalMaker. CrystalMaker Software Ltd, Begbroke, Oxfordshire, England. v10.6.3. **2014**.
16. Taylor R.; Wood P. A. *Chem. Rev.*. **2019**, *119 (16)*, 9427-9477.
17. Inorganic Crystal Structure Database ICSD. https://icsd. products.fiz-karlsruhe.de/
18. International Centre for Diffraction Data PDF. https://www. icdd.com/

19. The Rigaku Journal, *28(1),* **2012.**

20. Evans, J.S.O.; Evans, I.R.; *Chem. Soc. Rev*. **2004,** *33*, 539-547.

21. Dinnebier, R. E.; Billinge, S. J. Powder Diffraction: Theory and Practice; *RSC*. **2008**, 574.

22. Margiolaki I, Wright JP. Powder crystallography on macromolecules. *Acta Crystallogr A*. **2008**, *64*, 169–180.

23. West, A. R. *Basic Solid State Chemistry*, John Wiley & Sons: New York, **2000**.

24. Giacovazzo, C.; Monaco, H. L.; Viterbo, D.; Scordari, F.; Gilli, G.; Zanotti, G.; Catti, M. *Fundamentals of Crystallography*; Oxford University Press, **2002.**

25. Dinnebier, R. E.; Leineweber, A.; Evans, J. S. O. Rietveld Refinement, Practical Powder Diffraction Pattern Analysis using TOPAS; *De Gruyter*, **2018**, 331.

26. Evans, J. S. O.; Evans, I. R. *J. Chem. Educ*. **2021**, *98*, 495−505.

27. Le Bail, A. *Powder Diffraction*. **2005**, *20 (4)*, 316–326.

28. Friedrich, W.; Knipping, P.; von Laue, M. Interferenz-Erscheinungen bei Röntgenstrahlen. Bayer. *Akad. Wiss./Math.-Phys. Kl.: Sitzungsberichte*. **1912**, 303−322.

29. Rietveld, H. M. *J. Appl. Crystallogr*. **1969**, *2*, 65−71.

30. Runčevski**,** T.; Brown C. M.. *Cryst. Growth Des*. **2021**, *21*, 4821−4822.

31. David, W. I.; Shankland, K.; Baerlocher, C.; McCusker, L. Structure Determination from Powder Diffraction Data; Oxford University Press, **2002**.

32. David, W. I. F.; Shankland, K. *Acta Crystallogr., Sect. A*. **2008**, *64 (1)*, 52−64.

33. Schwartzenbach, D.; Abrahams, S. C.; Flack, H. D., Prince, E.; Wilson. A. J. C. Statistical descriptors in crystallography. II. Report of a working group on expression of uncertainty in measurement. *Acta Crystallogr., Sect. A: Found. Crystallogr*. **1995**, *51*, 565–569.

34. Prince, E. Mathematical Techniques in Crystallography and Materials Science 3rd ed. Springer, New York. **2004**.

35. Young, R. A. "Introduction to the Rietveld method," The Rietveld Method, edited by R. A. Young Oxford University Press, Oxford. **1993**. 1–38.

36. Young, R. A.; Sakthivel, A.; Moss, T. S.; Paiva-Santos, C. O. *J. Appl. Cryst.* **1995**, *28*, 366-367.

37. A.C. Larson, R.B. Von Dreele, General Structure Analysis System (GSAS); Report LAUR 86-748, Los Alamos National Laboratory, Los Alamos, NM. **2000**.

38. McCusker, L.B.; Von Dreele, R.; Cox, D. E.; Louer, D.; Scardi, P. *J. Appl. Crystallogr*. **1999**, *32 (1)*, 36−50.

39. Toby, B. H. *Powder Diffraction.* **2006**, *21 (1)*, 67–70.

40. Toby, B. H., *J. Appl. Crystallogr*. **2001,** *34*, 210-213.

41. Brown, P. J.; Matthewman, J. C. *Rutherford Appleton Lab. Rep.* **1987**, *RAL*, 87-010.

42. R-Carvajal, J. Recent Developments of the Program FULLPROF, in Commission on Powder Diffraction (IUCr) **2001**, *26*, 12.

43. Izumi, F. J. A software package for the Rietveld analysis of X-ray and neutron diffraction patterns.*Crystallogr. Ass Jpn*. v27, **1985**, 23-31.

44. Armstrong, A. R.; P. Anderson, A. *Inorg. Chem.* **1994**, *33 (19)*, 4366-4369.

45. Shannon, R. D.; Prewitt, C. T. *Acta Crystallogr.* **1969**, *B25*, 925-946.

46. Shannon, R. D. *Acta Crystallogr. Sect. A.* **1976,** *32*, 751-767.

47. Sato, M., Abo, J., Jin, T., & Ohta, M. *J. Alloys Compd.*, 192 (1–2). **1993**, 81-83.

48. Choi, J.; Zhang, X.; Wiley, J. B. *Inorg. Chem*. **2009** *48* (11), 4811-4816.

49. Viciu, L.; Koenig, J.; Spinu, L.; Zhou, W. L.; Wiley J. B. *Chemistry of Materials*. **2003** *15* (7), 1480-1485.

50. Ranmohotti, K. G. S.; Montasserasadi, M. D.; Choi, J.; Yao, Y.; Mohanty, D.; Josepha, E. A.; Adireddy, S.; Caruntu, G.; Wiley, J. B. *Mater. Res. Bull*. **2012**, 289-1294.